Hydrodynamic interaction of swimming organisms in an inertial regime

Gaojin Li, Anca Ostace, and Arezoo M. Ardekani

Phys. Rev. E **94**, 053104 — Published 4 November 2016

DOI: 10.1103/PhysRevE.94.053104

Hydrodynamic interaction of swimming organisms in an inertial regime

Gaojin Li[1], Anca Ostace[2] and Arezoo M. Ardekani[1],*
[1] *School of Mechanical Engineering, Purdue University, West Lafayette, IN 47907, USA*
[2] *Aerospace and Mechanical Engineering, University of Notre Dame, Notre Dame, IN 46556, USA*
(Dated: October 7, 2016)

We numerically investigate the hydrodynamic interaction of swimming organisms at small to intermediate Reynolds number regimes, i.e. $Re \sim$O(0.1-100), where inertial effects are important. The hydrodynamic interaction of swimming organisms in this regime is significantly different from the Stokes regime for microorganisms, as well as the high Reynolds number flows for fish and birds, which involves strong flow separation and detached vortex structures. Using an archetypal swimmer model, called "squirmer", we find that the inertial effects change the contact time and dispersion dynamics of a pair of pusher swimmers, and trigger hydrodynamic attraction for two pullers. These results are potentially important in investigating predator-prey interactions, sexual reproduction, encounter rate of marine organisms such as copepods, ctenophora, and larvae.

I. INTRODUCTION

Collective dynamics in microorganism suspensions, bird flocks and fish schools has received much attention in the past few years. These flows share many similarities despite the Reynolds number $Re = \rho U a/\mu$ ranging across several orders of magnitudes. Here U and a are the speed and length scale of the organism, ρ and μ are the density and dynamic viscosity of the surrounding fluid. The Reynolds number of typical swimmers are: $Re \sim 10^{-5}$ for bacteria, 10^{-3} for *Chlamydomonas*, $0.01 \sim 0.1$ for *Volvox* [1], 0.2 for *Paramecia* in the swimming mode and 2 in the escaping mode [2], 100 for *Pleurobrachia*, and $20 \sim 150$ for copepod [3]. Within the low Reynolds number regime ($Re = 10^{-5} \sim 10^{-3}$), bacteria in dense suspensions show a collective motion, including large-scale flow structures and vortices [4], locally correlated motions [5], spatial inhomogeneities of the swimmer distribution, and enhanced diffusion and mixing [6]. Similar phenomena were also observed in collective motions of microtubules [7], spermatozoa [8], self-motile colloidal particles [9] and vibrating granular systems [10]. At higher Reynolds numbers ($Re > 10^3$), the schools of fish and flocks of birds and insects are important for organisms to reduce the predation risk, to increase the success rate of feeding and reproduction [11]. At the base of each of these phenomena is the hydrodynamic interaction between the moving bodies and their detached vortical structures that leads to higher swimming (or flying) efficiency [12, 13].

The hydrodynamic interaction between microorganisms is essential to understand the dynamics of suspension of swimmers. In a dilute suspension, the leading-order effect of a freely swimming organism in Stokes regime behaves as a force dipole [14], whose induced velocity field decays as $1/r^2$. Based on the sign of the force dipole, microswimmers can be distinguished as pushers, which push the fluid away from the front and the back of their bodies, such as bacteria and spermatozoa, and pullers, which do the opposite, such as algae. The swimmer directly affects other cells by the induced velocity field and reorients their swimming direction by the induced velocity gradients. Even for two interacting microswimmers, the trajectories of the swimmers are strongly affected by the swimming mechanism, the relative displacement and orientation of the swimmers [15].

To fully understand the interaction between the microswimmers, it is important to consider the near-field hydrodynamics. The pairwise interaction between two swimmers is not negligible even at asymptotically large separations [16]. Experiments show that the cell-cell interaction between two swimming *Paramecia* is mainly governed by the hydrodynamic effects, rather than the biological interaction [2]. Two nearby *Volvox* colonies close to a solid surface are attracted toward each other and form stable bound states in which they dance around each other [1]. When in a suspension, the surface-mediated hydrodynamic interactions and the steric effects between the bacterial cells result in the formation of dynamic clusters and two-dimensional crystals [17, 18]. Many theoretical and numerical works have been conducted to investigate the hydrodynamic interactions between two model swimmers in the Stokes regime. Based on the squirmer model, which comprises a spherical body with a tangential surface deformation to generate swimming motion, both analysis and simulations show that the two pullers will first attract each other, then they dramatically change their orientation during the near contact and finally separate from each other [19]. Similar phenomena were also observed when including thermal fluctuations [20]. Two swimming bacteria, which use rotating helices to propel their cell bodies, considerably change their orientations and avoid each other [21]. When considering the details of the swimming stroke, the swimmer-swimmer interaction is complex depending on their relative displacement, orientation and phase, leading to different scattering angles [22, 23] and various types of motion, such as attraction, repulsion, or oscillation [24]. Another interesting phenomenon caused by the hydrodynamic interaction between two microswimmers is the enhancement of the swimming efficiency by

* ardekani@purdue.edu

synchronizing the phase of two adjacent flagella [25].

To the best of our knowledge all previous studies of interacting micro-organisms are limited to the Stokes regime. The inertial effects are important for many planktonic swimmers in the transition regime [26], such as copepods, larvae and *Pleurobrachia*. Inertial effects play an important role in changing swimming direction of small organisms, attacking a prey, or escaping from a predator. For example, copepod *nauplii* exhibit unsteady motion during escaping mode and the Reynolds number is about 6 [27]. In our previous studies, we have shown that the small but finite inertia causes a dramatic change to the near-wall motion of a swimmer [28] and the biogenic mixing efficiency [29]. One of the key differences due to the inertial effects is that the linearity of the governing equations in the Stokes regime breaks. Also, contrary to the zero Reynolds number regime, where the input power is fully dissipated into the surrounding fluid, in the inertial regime part of the power is used to accelerate the body.

In this work, we examine the hydrodynamic interaction of model swimmers in the small to intermediate Reynolds number regime, by means of direct numerical simulations. The inertial effects cause a significant change in the contact time and dispersion dynamics of swimmers. The results are helpful in better understanding the organisms encounter dynamics and their collective behavior.

II. GOVERNING EQUATIONS AND NUMERICAL METHODS

The Navier-Stokes equations for an incompressible Newtonian fluid are solved in the entire computational domain

$$\rho\frac{D\boldsymbol{u}}{Dt} = -\nabla p + \nabla^2\boldsymbol{u} + \boldsymbol{f}, \tag{1a}$$

$$\nabla\cdot\boldsymbol{u} = 0, \tag{1b}$$

where $\boldsymbol{u}$ is the velocity, p is the pressure, and μ is the viscosity. The density ρ is equal to the swimmer density ρ_p inside the squirmer and equal to the fluid density ρ_f in the fluid domain. In this study, we set $\rho_p = \rho_f$ since the density of organisms is usually close to the background fluid. The swimmer is resolved by adding a forcing term inside the swimmer body using a distributed Lagrangian multiplier method [30], which is calculated by iteration as

$$\boldsymbol{f} = \boldsymbol{f}^* + \alpha\frac{\rho\phi}{\Delta t}(\boldsymbol{U} + \boldsymbol{\Omega}\times\boldsymbol{r} + \boldsymbol{u}_i - \boldsymbol{u}), \tag{2}$$

where $\boldsymbol{U}$ is the translational velocity of the squirmer, $\boldsymbol{\Omega}$ is the angular velocity, $\boldsymbol{u}_i$ is the imposed velocity causing the self-propulsion, $\boldsymbol{f}^*$ is the force calculated in the previous iteration, α is a dimensionless factor whose value affects the convergence rate but not the solution, ϕ is the volume fraction occupied by the swimmer in each computational grid ($\phi = 1$ inside, $\phi = 0$ outside and $0 < \phi < 1$ for the grids at the surface of the swimmer).

The squirmer model is introduced by Lighthill [31] and Blake [32] and has been historically used for swimmers in the Stokes regime such as Volvox. However, more recently squirmer model has been extended to low and intermediate Reynolds number regimes [28, 29, 33–36]. This swimming model is the first step in understating the effects of inertia and can predict the behavior of large ciliates in oceans and lakes such as *Pleurobrachia*. We consider the first two squirming modes and consequently the magnitude of the tangential velocity on the squirmer surface is written as

$$u_\theta^s(\theta) = B_1\sin\theta + B_2\sin\theta\cos\theta, \tag{3}$$

where θ is the polar angle measured from the swimming direction, B_1 and B_2 are the first two squirming modes. The parameter $\beta = B_2/B_1$ distinguishes pullers ($\beta > 0$) and pushers ($\beta < 0$). In the Stokes regime, the swimming speed of a squirmer in an unbounded domain is $U_0 = 2B_1/3$. To recover the tangential velocity u_θ^s on the surface of the squirmer, we impose the following solenoidal velocity $\boldsymbol{u}_i$ inside the squirmer

$$\begin{aligned}\boldsymbol{u}_i = &\left[\left(\frac{r}{a}\right)^m - \left(\frac{r}{a}\right)^{m+1}\right](u_s\cot\theta + \frac{du_s}{d\theta})\boldsymbol{e}_r \\ &+ \left[(m+3)\left(\frac{r}{a}\right)^{m+1} - (m+2)\left(\frac{r}{a}\right)^m\right]u_s^\theta\boldsymbol{e}_\theta,\end{aligned} \tag{4}$$

where a is the radius of the squirmer, $\boldsymbol{e}_r$ and $\boldsymbol{e}_\theta$ are the unit vectors along r and θ directions, m is an arbitrary positive integer, where the simulation results are independent of its value. The particle translational and angular velocities are calculated as

$$\boldsymbol{U} = \frac{1}{M_p}\int_{V_p}\rho_p(\boldsymbol{u} - \boldsymbol{u}_i)dV, \tag{5}$$

$$\mathbf{I}_p\boldsymbol{\Omega} = \int_{V_p}\rho_p\boldsymbol{r}\times(\boldsymbol{u} - \boldsymbol{u}_i)dV, \tag{6}$$

where V_p, M_p and $\mathbf{I}_p$ are the volume, mass and moment of inertia of the particle. Iterations are repeated until the maximum of Euclidean norm of $(\boldsymbol{f} - \boldsymbol{f}^*)/\boldsymbol{f}$ and the normalized residual fall below the specified tolerance of 10^{-3}.

When the squirmer approaches another squirmer, the high pressure in the thin film between the squirmers prevents any unphysical overlaps. However, a very small grid resolution is needed to resolve the thin liquid film and consequently it is computationally expensive. A repulsive force is imposed during the collision to prevent the unphysical overlap [37]:

$$\boldsymbol{F}_r = \frac{C_m}{\varepsilon}\left(\frac{d - d_{min} - dr}{dr}\right)^2\boldsymbol{e}, \tag{7}$$

where $C_m = M_pU_0^2/a$ is the characteristic force, $\varepsilon = 10^{-4}$ is a small positive number, d is the distance between two

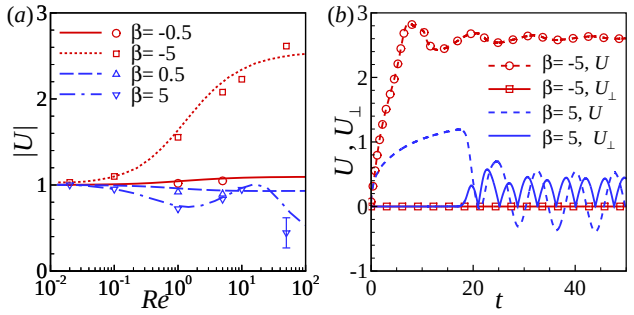

FIG. 1. (Color online) (a) Swimming speed of a squirmer of $\beta = \pm 0.5$ and ± 5 at different Reynolds numbers. The symbols show the current results, and lines show previously published simulation results for a squirmer with a fixed orientation [36]. (b) Time history of the velocity components of a single squirmer of $\beta = \pm 5$ at $Re = 50$. $U_\perp$ represents the velocity component perpendicular to the direction of squirmer's orientation.

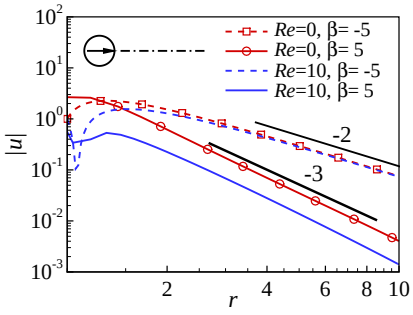

FIG. 2. (Color online) Velocity magnitude away from an isolated squirmer at $Re = 0$ and 10 along the swimming direction.

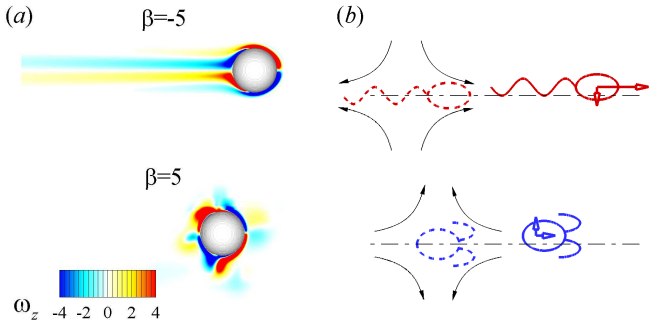

FIG. 3. (Color online) (a) Vorticity field ω_z around a single pusher of $\beta = -5$ (top) and puller of $\beta = 5$ (bottom) at $Re = 50$. (b) Schematic representation of inertial effects on the swimming motion of a single pusher and puller.

squirmers, $d_{min} = 2a$ is the minimum possible distance, dr is the force range and is set to be twice the smallest grid size Δ. The direction of the repulsive force $\boldsymbol{e}$ is along the line of center of the two squirmers.

Simulations are conducted using a finite volume method on a fixed staggered grid implemented in the code developed by Sadegh Dabiri and coworkers [38–40]. A conventional operator splitting method is applied to enforce the continuity equation. The second-order TVD (total variation diminishing) Runge-Kutta method is used for time marching. The spatial derivatives in the convection term are evaluated using the QUICK (Quadratic Upstream Interpolation for Convective Kinetics) scheme and the diffusion terms are discretized using the central difference scheme. The results are normalized by the characteristic length a, velocity $U_0 = 2B_1/3$ and time a/U_0. The mesh size and time step are $\Delta = 0.06$ and $\Delta t = 2.5\times10^{-4}$ for all the cases, except for $Re = 0.1$, where we use $\Delta = 0.1$ and $\Delta t = 10^{-3}$, and the diffusion terms are implicitly solved. Validation of the numerical method and the convergence studies are given in sections III A and III B. Additional validation and verification tests using this code can be found in our previous publications [28, 29, 41, 42].

III. RESULTS

A. Swimming motion of a single squirmer

The motion of a single squirmer in an unbounded fluid is first investigated. Fig. 1(a) shows the magnitude of the swimming speed at various Reynolds numbers. A pusher swims faster while a puller swims slower with increasing Re. From the perturbation theory [34], the swimming speed of a squirmer in an unbounded domain is $U \approx 1 - 0.15\beta Re$ and holds well for $Re < 0.1$ [28]. Our results agree with the previous simulations [36] for pushers and for pullers at $Re < 10$. At higher Re, the puller becomes unstable and the previous results of a squirmer with a fixed orientation [36] does not describe the behavior of a freely swimming squirmer. The swimming motion of a pusher is always stable in the range of Reynolds number investigated in this manuscript. The velocity field around a squirmer at finite Reynolds number decays as $|u| \sim r^{-3}$ and is faster than a squirmer in a Stokes flow which behaves as a force dipole $|u| \sim r^{-2}$ (see figure 2). Velocity decay of swimming zooplankton, such as *Mesodinium rubrum* and *Podon intermedius* is closer to an inertial squirmer than a Stokes squirmer [43].

Fig. 1(b) shows the time history of a single squirmer of $\beta = \pm 5$ at $Re = 50$. For a pusher, the initial oscillation in the speed eventually dampens out and it will swim with a constant speed. A pusher has a long vorticity wake as shown in Fig. 3(a). In contrast, the swimming motion of a puller becomes unstable at $Re \sim 10$, leading to a three dimensional swimming trajectory. The vorticity field is also more complex for an unstable puller. These observations can be explained by the following arguments. With increasing Re, the history effects become important and the swimmer is more affected by the flow field induced

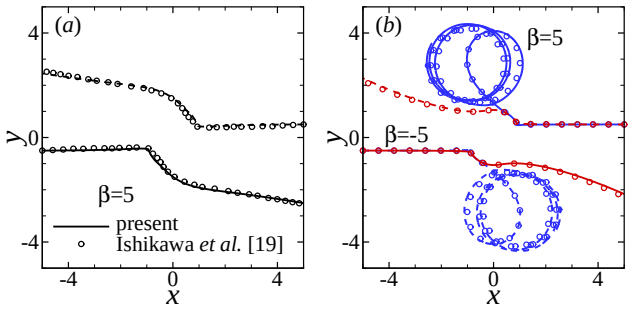

FIG. 4. (Color online) (a) Comparison of the trajectories of two colliding pullers. Present results correspond to $Re = 0.1$ and previous results are obtained for Stokes flow [19]. (b) Comparison of the trajectories of two squirmers at $Re = 10$ using different gird resolutions, $\Delta = 0.06$ (line) and 0.04 (symbols).

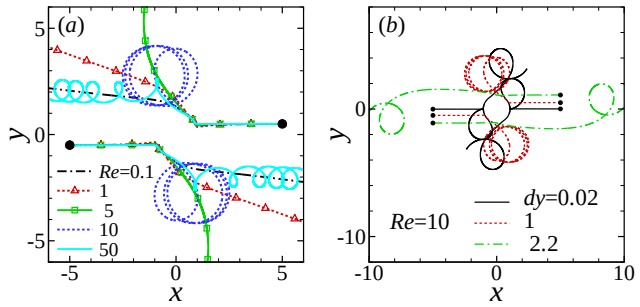

FIG. 5. (Color online) (a) Trajectories of two pullers of $\beta = 5$ at different Reynolds numbers. (b) Trajectories of two pullers at $Re = 10$ and different dy.

by itself at a previous time (see Fig. 3(b)). The pusher is "pushed" to swim faster due to the velocity field induced by itself at an earlier time (dashed swimmer), while the puller is "pulled" and swims slower. The stability of the swimmer is also related to the hydrodynamic interaction between its body and the velocity field created by its movement. A pusher will return to its original trajectory due to the hydrodynamic attraction if it is laterally perturbed away from the straight trajectory. The response of a puller is exactly opposite, and its trajectory becomes unstable with increasing inertial effect.

B. Pair-wise interaction of two pullers

In this section, we consider the pair-wise interactions of two pushers ($\beta = -5$) and two pullers ($\beta = 5$) which are initially located in the same plane ($z = 0$). They initially swim towards each other and their swimming orientations are initially parallel. The distance between their centers is dx and dy in the x and y directions, respectively. We set $dx = 10$ and $dy = 1$ unless otherwise mentioned. As shown in Fig. 4(a), our results of two pullers at $Re = 0.1$ agree well with the previous results [19] in the Stokes regime. Further, convergence studies performed for squirmers at higher Reynolds number ($Re = 10$) show that the results are independent of mesh size (see Fig. 4(b)).

The hydrodynamic interaction of two pullers are dramatically modified due to the presence of inertia. The comparison of the trajectories of two pullers at different Reynolds numbers are shown in Fig. 5(a). Fig. 6 shows the time evolution of the flow field and the pullers' swimming trajectories at different Reynolds numbers. At $Re = 0.1$ and 1, the two pullers rotate away from each other during the collision and eventually escape with positive scattering angles. The recirculating regions with high vorticity value ω_z in front of and behind an isolated swimmer at $Re = 0.1$ have similar shape and size (see Fig. 6($a1$)). At higher Reynolds numbers, the pullers generate larger recirculating regions behind their body, which are similar to the ones observed for a cruising *Metridia longa* [43]. The rotation of the swimmer is so strong that the trajectories become circular after the separation. The vorticity field is strongly disturbed due to the spinning motion of the pullers (see Fig. 6($b1 - b4$) and ($c1 - c4$)). Notably, the two pullers at $Re = 10$ are hydrodynamically entrapped near each other as they are rotating in circular trajectories for a long time. At $Re = 50$, the two pullers swim away from each other following circular trajectories with small radii of curvature. The trajectories of two pullers at $Re = 10$ under different initial configurations $dy = 0.02$ and $dy = 2.2$ are plotted in Fig. 5(b). It is clear that the details of trajectories are closely related to the initial condition, but the hydrodynamic entrapment in circular trajectories exists for different Reynolds numbers above $Re \sim 10$ and different initial lateral distances. These observations are qualitatively similar to the bound states of two dancing spherical alga *Volvox* near a surface [1]. However, the mechanisms in the two cases are very different. The corresponding Reynolds number of a *Volvox* is around 0.03, and the formation of a bound state occurs due to the Volvox swimming motion near a boundary. Here, the inertial effects lead to the instability of the swimming motion of a single puller as discussed in section III A, which dramatically modifies the hydrodynamic interaction between the two swimmers.

Fig. 7 shows the time evolution of the U-velocity component and the angular velocity Ω_z of the pullers at different Reynolds numbers. The U-velocity of the pullers quickly drops during the collision and then it recovers and reaches to a peak value. After they separate from each other, the puller at low Re swims with a roughly constant speed, which is reduced compared to the swimming speed of a single squirmer due to the flow field induced by the other squirmer. At higher Re, the U-velocity oscillates. The pullers always rotate in a clockwise direction during the collision as shown in Fig. 7(b). The vorticity in the gap region between the two swimmers is first negative as the swimmers get close to each other (see Fig.

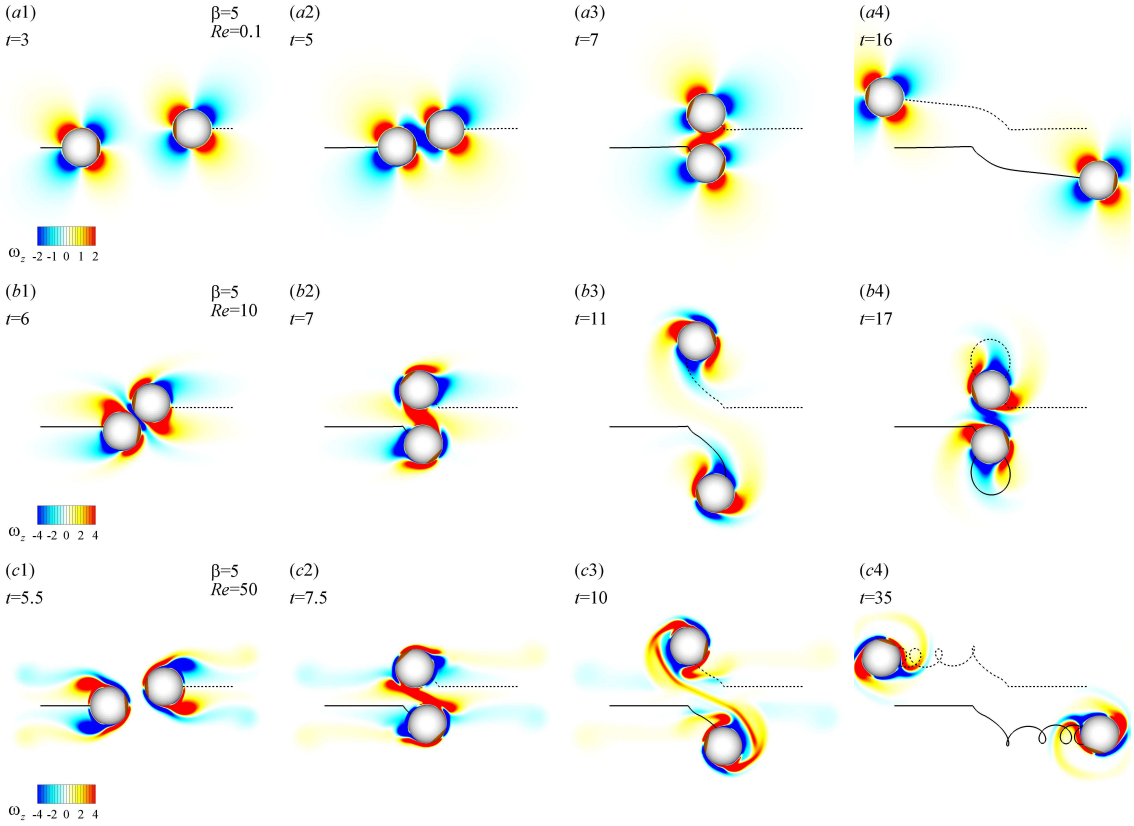

FIG. 6. (Color online) Time sequence of the swimming motion of two pullers of $\beta = 5$ at $(a1 - a4)$ $Re = 0.1$, $(b1 - b4)$ $Re = 10$ and $(c1 - c4)$ $Re = 50$. The contour plots show the vorticity ω_z in the plane $z = 0$. The black lines show the trajectories of the swimmers. For movies see [46].

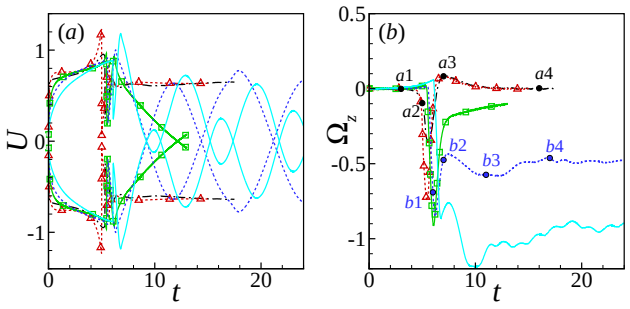

FIG. 7. (Color online) Time history of (a) U-velocity component and (b) angular velocity Ω_z of two pullers of $\beta = 5$ at different Reynolds numbers. Legends are the same as Fig. $5(a)$.

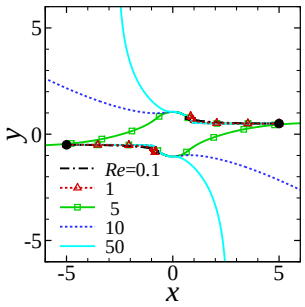

FIG. 8. (Color online) Trajectories of two pushers of $\beta = -5$ at different Reynolds numbers.

$6(a2)$). Then the magnitude of Ω_z decreases after the two swimmers pass each other (see Fig. $6(a4)$). At low Re, the angular velocity becomes positive due to the strong induced rotating effects from the vorticity field, it then gradually goes to zero as the two swimmers separate from each other. At high Re, the inertial effects greatly enhance the initial rotation in the clockwise direction, the pullers maintain a high angular velocity after their separation and swim in circular trajectories.

C. Pair-wise interaction of two pushers

In Fig. 8, we compare the trajectories of two pushers of $\beta = -5$ at different Reynolds numbers. Their flow

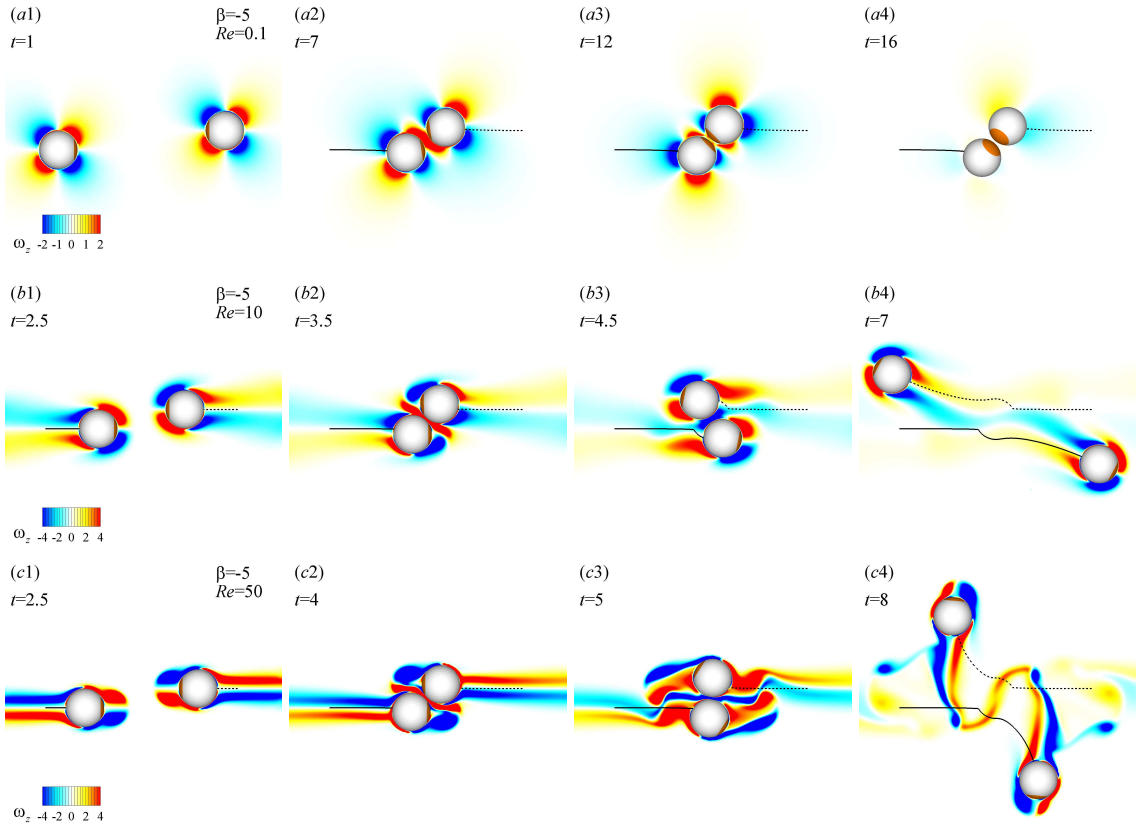

FIG. 9. (Color online) Time sequence of the swimming motion of two pushers of $\beta = -5$ at $(a1-a4)$ $Re = 0.1$, $(b1-b4)$ $Re = 10$ and $(c1-c4)$ $Re = 50$. The contour plots show the vorticity ω_z in the plane $z = 0$. The black lines show the trajectories of the swimmers. For movies see [46].

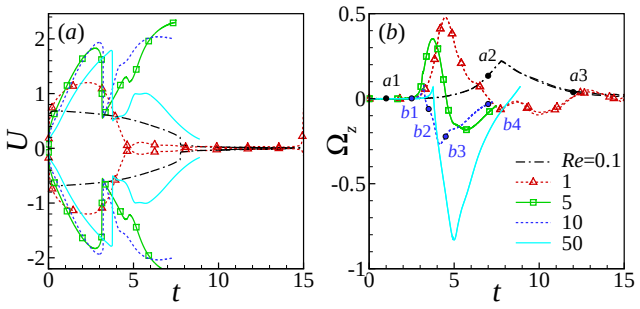

FIG. 10. (Color online) Time history of (a) U-velocity component and (b) angular velocity Ω_z of two pushers of $\beta = -5$ at different Reynolds numbers.

fields are shown in Fig 9. At $Re = 0.1$, the two pushers stay in close contact for a long time after the collision. Meanwhile, they rotate towards each other and get trapped. This state is unstable, the two pushers eventually swim away and leave their initial swimming plane. At higher Reynolds numbers, the squirmers keep swimming in their initial plane after collision, and the scattering angle strongly depends on the Reynolds number. At $Re = 5$, the scattering angle is negative, while at $Re = 50$, the scattering angle is almost positive 90 degrees. A long vorticity wake is formed behind the pushers at $Re = 10$ and 50 as shown in Fig. 9, where its magnitude is stronger than the wake vorticity at $Re = 0.1$. After the two pushers pass each other, their vorticity wakes have strong effects on their motion, causing them to rotate in a clockwise direction. The interaction between the two wakes is stronger at higher Re. As seen in Fig. 9$(c4)$, the elongated wakes become unstable and generate ring-like vortical structures in three dimensions.

The U-velocity and the angular velocity Ω_z of the pushers are shown in Fig. 10. At $Re = 0.1$, the swimming speed of the pushers gradually decreases as they approach each other. As the swimmers get close, they lose enough momentum and are not able to pass each other. Meanwhile, the swimmers keep rotating in a counterclockwise direction before their heads-on collision. They spend a long time in the heads-on configuration till eventually small perturbations lead to their reorientation and they eventually escape. At higher Reynolds numbers $(Re = 10, 50)$, the pushers swim much faster and their angular velocity only slightly increases before they collide. The swimmers at higher Reynolds numbers maintain a

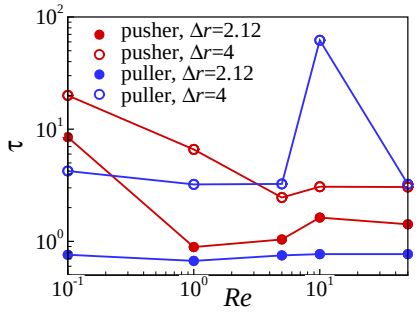

FIG. 11. (Color online) Contact ($\Delta r \leq 2.12$) and near-by ($\Delta r \leq 4$) time τ of two squirmers of $\beta = \pm 5$ at different Reynolds numbers.

high momentum before collision and they easily pass each other. The inertial effects also cause the swimmers to rotate in a clockwise direction (Fig. 9($b2$)) as opposed to courter-clockwise rotation in the low Reynolds number regime (Fig. 9($a2$)). Eventually, the two swimmers escape from each other staying in their initial plane.

D. Contact time of two swimmers

In Fig. 11, we quantify the inertial effects on the contact time τ of the two squirmers. The contact time is defined as the time duration when the distance between the center of the squirmers is smaller than $\Delta r = 2.12$, where the repulsive collision force is non-zero. The collision time is greatly reduced for pushers at higher Re, while it is less affected for pullers. We also define the nearby time which is the time duration when the distance between the center of squirmers is smaller than twice their diameter. For the pushers, the same trend is observed for the near-by time as the contact time. For the pullers, nearby time is affected due to the entrapment of the pullers in a circular loop. The two pullers at $Re = 10$ stay around each other for a much longer time. These results are important in estimating the encounter time for organisms, which is important in reproduction, feeding and escaping from a predator. For example, experiments show that the male calanoid copepod species *T. longicornis* locate and pursue females within twice the body length of a female's swimming path following odour tracers [44]. They accelerate and the Reynolds number changes from 5−15 in a normal swimming mode to 20−40 in a pursuit [45]. In this example, both their hydrodynamic interaction and the evolution of the odour tracers are greatly affected by the inertial effects.

IV. CONCLUSIONS

In this study, we numerically investigated the effects of inertia on the swimming motion and the pair-wise hydrodynamic interactions of small organisms. The squirmer model is used, representing two types of swimming strategies typically encountered in motile cells: pullers and pushers. With increasing Re, a squirmer interacts with the flow field induced by itself at an earlier time. As a result, a pusher swims faster in a straight line, while a puller swims slower and its swimming trajectory is unstable. The contact time of two interacting pushers is reduced by increasing inertial effects, In contrast, a pair of pullers at $Re \sim 10$ are hydrodynamically bounded in circular trajectories near each other. The pair-wise interaction of organisms is the first critical step to gain fundamental understanding of the collective behavior of small organisms. Our results show that the inertial effects can greatly affect the decisive biophysical interactions of small organisms. In this work, we focus on the inertial effects on the swimmer, and the swimmer model is simplified to have a tractable number of parameters in the problem. While in nature, the swimming motion of many organisms are highly unsteady. Previous studies have used a squirmer model with an unsteady slip velocity [33, 47], which involves more parameters in the physical space. The details of the unsteadiness and the swimming kinematics could have important effects on the hydrodynamic interaction of swimmers. Further studies are required to include these effects.

V. ACKNOWLEDGEMENTS

This publication was made possible, in part, with support from NSF (Grant No. CBET-1445955-CAREER). Anca Ostace acknowledges the Martin and Carmel Naughton Graduate Fellowship.

[1] K. Drescher, K. C. Leptos, I. Tuval, T. Ishikawa, T. J. Pedley, and R. E. Goldstein, Phys. Rev. Lett. **102**, 168101 (2009).
[2] T. Ishikawa and M. Hota, J. Exp. Biol. **209**, 4452 (2006).
[3] T. Kiørboe, H. Jiang, and S. P. Colin, Proc R Soc Lond [Biol] , rspb20100629 (2010).
[4] C. Dombrowski, L. Cisneros, S. Chatkaew, R. E. Goldstein, and J. O. Kessler, Phys. Rev. Lett. **93**, 098103 (2004).
[5] A. Sokolov, I. S. Aranson, J. O. Kessler, and R. E. Goldstein, Phys. Rev. Lett. **98**, 158102 (2007).
[6] X. L. Wu and A. Libchaber, Phys. Rev. Lett. **84**, 3017 (2000).
[7] Y. Sumino, K. Nagai, Y. Shitaka, D. Tanaka, K. Yoshikawa, H. Chaté, and K. Oiwa, Nature **483**, 448 (2012).

[8] I. Riedel, K. Kruse, and J. Howard, Science **309**, 300 (2005).
[9] J. R. Howse, R. A. L. Jones, A. J. Ryan, T. Gough, R. Vafabakhsh, and R. E. Golestanian, Phys. Rev. Lett. **99**, 048102 (2007).
[10] V. Narayan, S. Ramaswamy, and N. Menon, Science **317**, 105 (2007).
[11] M. Milinski and R. Heller, Nature **275** (1978).
[12] F. Fish, J. Exp. Zool. **273**, 1 (1995).
[13] A. Becker, H. Masoud, J. Newbolt, M. Shelley, and L. Ristroph, Nat. Commun. **6** (2015).
[14] A. Chwang and T. Wu, J. Fluid Mech. **67**, 787 (1975).
[15] E. Lauga and T. Powers, Rep. Prog. Phys. **72**, 096601 (2009).
[16] R. Clarke, M. Finn, and M. MacDonald (The Royal Society, 2014) p. 20130508.
[17] X. Chen, X. Yang, M. Yang, and H. Zhang, Europhys. Lett. **111**, 54002 (2015).
[18] A. P. Petroff, X.-L. Wu, and A. Libchaber, Phys. Rev. Lett. **114**, 158102 (2015).
[19] T. Ishikawa, M. Simmonds, and T. Pedley, J. Fluid Mech. **568**, 119 (2006).
[20] I. O. Götze and G. Gompper, Phys. Rev. E **82**, 041921 (2010).
[21] T. Ishikawa, G. Sekiya, Y. Imai, and T. Yamaguchi, Biophys. J. **93**, 2217 (2007).
[22] G. P. Alexander, C. M. Pooley, and J. M. Yeomans, Phys. Rev. E **78**, 045302 (2008).
[23] A. Furukawa, D. Marenduzzo, and M. E. Cates, Phys. Rev. E **90**, 022303 (2014).
[24] C. M. Pooley, G. P. Alexander, and J. M. Yeomans, Phys. Rev. Lett. **99**, 228103 (2007).
[25] G. J. Elfring and E. Lauga, Phys. Rev. Lett. **103**, 088101 (2009).
[26] J. Yen, Biol. Bull. **198**, 213 (2000).
[27] B. Gemmell, J. Sheng, and E. Buskey, Proc. Natl. Acad. Sci. U.S.A. **110**, 4661 (2013).
[28] G. Li and A. M. Ardekani, Phys. Rev. E **90**, 013010 (2014).
[29] S. Wang and A. Ardekani, Sci. Rep. **5** (2015).
[30] A. Ardekani, S. Dabiri, and R. Rangel, J. Comput. Phys. **227**, 10094 (2008).
[31] M. Lighthill, Comm. Pure Appl. Math. **5**, 109 (1952).
[32] J. Blake, J. Fluid Mech. **46**, 199 (1971).
[33] S. Wang and A. Ardekani, J. Fluid Mech. **702**, 286 (2012).
[34] S. Wang and A. Ardekani, Phys. Fluids **24**, 101902 (2012).
[35] A. Doostmohammadi, R. Stocker, and A. M. Ardekani, Proc. Natl. Acad. Sci. U.S.A. **109**, 3856 (2012).
[36] N. Chisholm, D. Legendre, E. Lauga, and A. Khair, J. Fluid Mech. **796**, 233 (2016).
[37] R. Glowinski, T. Pan, T. Hesla, D. Joseph, and J. Periaux, J. Comput. Phys. **169**, 363 (2001).
[38] S. Dabiri, J. Lu, and G. Tryggvason, Phys. Fluids **25**, 102110 (2013).
[39] S. Dabiri and G. Tryggvason, Chem. Eng. Sci. **122**, 106 (2015).
[40] S. Dabiri, A. Doostmohammadi, M. Bayareh, and A. Ardekani, Int. J. Multiph. Flow **69**, 8 (2015).
[41] G. Li, A. Karimi, and A. Ardekani, Rheol. Acta **53**, 911 (2014).
[42] G. Li, G. McKinley, and A. Ardekani, J. Fluid Mech. **785**, 486 (2015).
[43] T. Kiørboe, H. Jiang, R. J. Gonçalves, L. T. Nielsen, and N. Wadhwa, Proc. Natl. Acad. Sci. U.S.A. **111**, 11738 (2014).
[44] M. Weissburg, M. Doall, and J. Yen, Phil. Trans. R. Soc. B **353**, 701 (1998).
[45] M. Doall, S. Colin, J. Strickler, and J. Yen, Phil. Trans. R. Soc. B **353**, 681 (1998).
[46] Supplementary Material at [] for the videos of two interacting pushers and pullers.
[47] V. Magar and T. Pedley, J. Fluid Mech. **539**, 93 (2005).